inorganics

MDPI

Article

Sodium Methoxide/Zeolite-Supported Catalyst for Transesterification of Soybean Waste Cooking Oil for Biodiesel Production

Kidist Argaw Shiferaw †, Joshua Manoj Mathews †, Eunsu Yu, Eun-Young Choi and Naresh Hiralal Tarte *,†

Korea Science Academy of KAIST, Busan 47162, Republic of Korea
* Correspondence: naresh@kaist.edu; Tel.: +82-51-606-2276
† These authors contributed equally to this work.

Abstract: This study aims to prepare a supported catalyst based on zeolite Y doped with NaOMe (sodium methoxide) for the transesterification of waste cooking oil (WCO). The catalytic screening data showed that NaOMe/zeolite is a prominent catalyst for the transesterification of WCO prepared by a solvent-free, ball-milling process. We initially tested 5–20% of sodium methoxide loading onto zeolite Y and found that 20% is the optimum loading for the reaction. The transesterification reaction required a comparatively lower methanol-to-oil mole ratio of 16:1 with the reaction temperature as 60 °C. The ball-milled NaOMe/zeolite catalyst was characterized by BET surface area analysis, FE-SEM, TEM, FT−IR, and XRD. The BET surface analysis revealed that the surface area for zeolite Y was substantially decreased in the NaOMe/zeolite catalyst. The ball-milling process dropped the crystallinity of zeolite Y, which can be seen from the XRD and FE-SEM images of both zeolite Y and the NaOMe/zeolite catalyst. Finally, the transesterification reaction product was fully characterized by ^{1}H-NMR and viscosity analysis for biodiesel, glycerol, and the WCO. The chemical shifts for the biodiesel and glycerol are found accordingly. This is also supported by the FT−IR characterization of biodiesel, glycerol, and WCO. It is noteworthy that a very high mass ratio of 250 g oil/g NaOMe is obtained when converting WCO to biodiesel, indicating very high catalytic activity for the aforementioned catalyst.

Keywords: biodiesel; transesterification; catalyst; sodium methoxide; ^{1}H-NMR

Citation: Argaw Shiferaw, K.; Mathews, J.M.; Yu, E.; Choi, E.-Y.; Tarte, N.H. Sodium Methoxide/Zeolite-Supported Catalyst for Transesterification of Soybean Waste Cooking Oil for Biodiesel Production. *Inorganics* **2023**, *11*, 163. https://doi.org/10.3390/inorganics11040163

Academic Editors: Franz Edwin López Suárez, Robison Buitrago and Andres F. Suárez

Received: 13 December 2022
Revised: 4 April 2023
Accepted: 6 April 2023
Published: 12 April 2023

1. Introduction

On 1 January 2016, the United Nations announced the first goal that we as humans should pursue to transform our world so that each person gets the opportunity to experience health, justice, and prosperity by 2030 [1]. At the present time, as we are moving forward to a technologically advanced future, our energy consumption has risen exponentially [2]. Due to fossil fuels such as petroleum and diesel being nonrenewable energy sources and contributing to the release of greenhouse gasses, researchers have started siding with alternative energy sources [3–7].

Currently, waste cooking oil, the byproduct of many food industries, is mainly produced by the US, followed by China and then European countries. According to references, the worldwide availability of WCO in the market is roughly 20 million tons per year [8]. Presently, developed countries are recycling waste products such as waste cooking oil (WCO) to biodiesel not only as a means of proper waste management but also to decrease their carbon footprint [8–10].

In the present day, there are two mechanisms used to convert WCO to usable biodiesel. One method uses transesterification, and the other uses hydrotreating. The hydrotreating process involves a specific catalyst operated under a very high temperature and pressure of hydrogen gas, which is not economically friendly in comparison to transesterification [5,11–13]. Despite the fact that homogeneous catalysts are corrosive and their

separation from the final product is a difficult process, they are widely used as a catalyst for the transesterification of WCO [3,14]. Further investigation in this sector shows that heterogeneous catalysts are more advantageous as the biodiesel and glycerol products can easily be separated by phase separation [14–20]. The sediment of the catalyst can also be reused again, thus being eco-friendly in nature and economically efficient.

During the process of frying, WCO with a triglyceride backbone experiences an ester bond breakage at a high temperature, producing free fatty acid (FFA) [21–23]. The moisture from the vegetables also results in the hydrolysis of triglyceride-producing FFA [24]. The presence of FFA in WCO and the use of a large amount of catalyst will lead to a disadvantageous saponification reaction; hence, it is necessary to remove FFA before the transesterification of WCO [3]. Zeolites are well known for their abilities of ion exchange and reversible dehydration [16,25]. Hence, the pretreatment process for the removal of FFA from WCO may be avoided while using a zeolite-based catalyst for the transesterification reaction [16,26,27]. Zeolite Y has already been used for the transesterification of WCO; however, only a maximum biodiesel yield of about 25% could be achieved [16,28].

Out of the many problems that the biodiesel industry is facing, the costly process of pre-treating WCO and the inefficient production of biodiesel can be considered the most significant ones [29]. The main purpose of this research work is to find a suitable catalyst to make the conversion from WCO to biodiesel much cheaper and easier. Despite the relatively large amount of NaOMe used as a catalyst for the production of biodiesel, combining it with zeolite Y will make it more beneficial in wider aspects. Hence, we propose a new catalyst, NaOMe/zeolite synthesized by a solvent-free, ball-milling process for the conversion of WCO to biodiesel without the pre-treatment of WCO, which allows us to successfully avoid saponification.

2. Results and Discussion

2.1. Catalyst Characterization

2.1.1. Fourier Transform Infrared Spectroscopy (FT−IR)

To confirm the presence of both NaOMe and zeolite Y in the synthesized catalyst, FT−IR analysis was performed, and the resulting peaks implied their incorporation. The Fourier transform infrared spectra of the NaOMe/zeolite catalyst, NaOMe, and zeolite Y are depicted in Figure 1. The FT−IR, as shown in the figure, was obtained in the region of 650–4000 cm^{-1} with 5 cm^{-1} of resolution to observe the structural vibrations of zeolite Y and the doped NaOMe/zeolite catalyst along with pure NaOMe at room temperature. The peak observed at 959 cm^{-1} indicates the presence of Si-OH and SiO-Al bonds, as well as Al-OH bonds [30]. Additionally, it corresponds to the asymmetric and symmetric stretching vibrations of the internal MO_4 structure, where M refers to either silica or aluminum [30]. The bands at 1132 cm^{-1} and 775 cm^{-1} correspond to the external MO_4 structure's asymmetric and symmetric stretching vibrations, respectively [30]. The peak at 1362 cm^{-1} is attributed to the double-ring external link that is associated with the FAU structure [30]. FT−IR analysis conducted on NaOMe revealed the presence of asymmetric and symmetric C-H stretching vibrations at 2832 cm^{-1} and 2773 cm^{-1}, respectively. Furthermore, C-O stretching vibrations were visible at 1633 cm^{-1}, and C-O-Na bending vibrations occurred at 1433 cm^{-1}. Additionally, the H-C-H wagging and rocking vibrations were observed at 775 cm^{-1} and 881 cm^{-1}, respectively. These vibrations are also present in the NaOMe/zeolite catalyst.

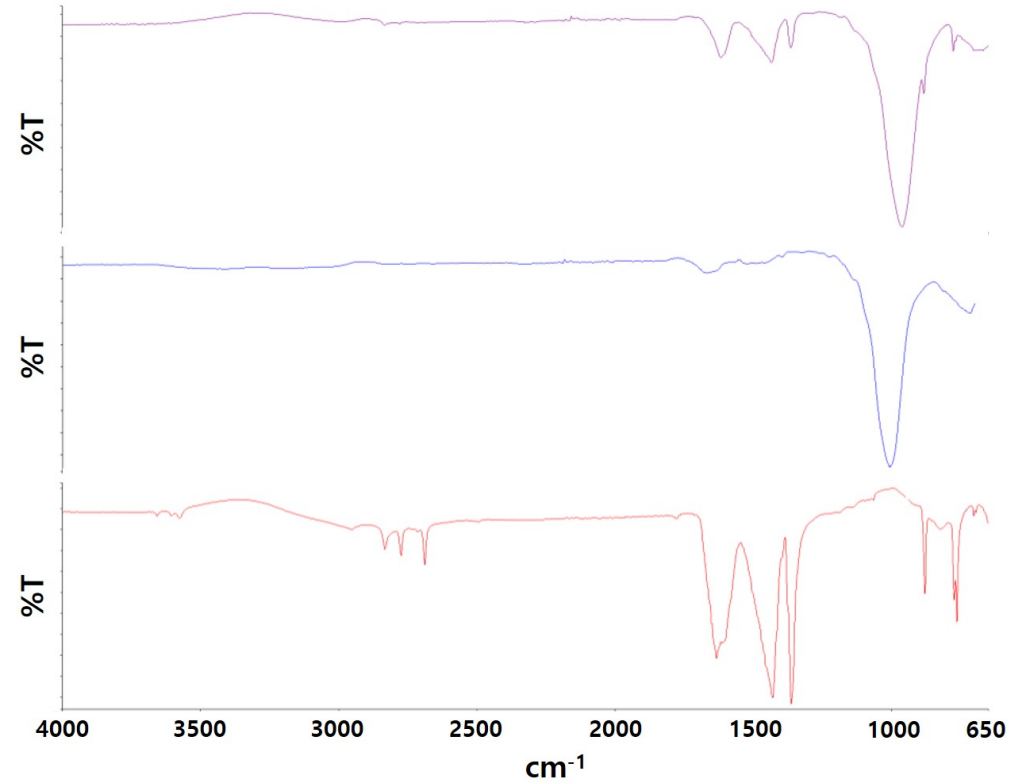

Figure 1. FT−IR spectrum of NaOMe/zeolite catalyst in comparison to NaOMe and zeolite.

2.1.2. X-ray Diffraction (XRD)

The crystallinity and diffraction pattern was confirmed by the pattern in the known reference zeolite Y [31]. There is a drastic decrease in the crystallinity that was observed in the ball-milled sample, which is supported by the SEM images in Figure 2. The loss of crystallinity was also reported in the dry, ball-milling process of zeolite Y, which ultimately resulted in nanoparticles [32]. This also occurred with the clay-based NaOMe catalyst [33].

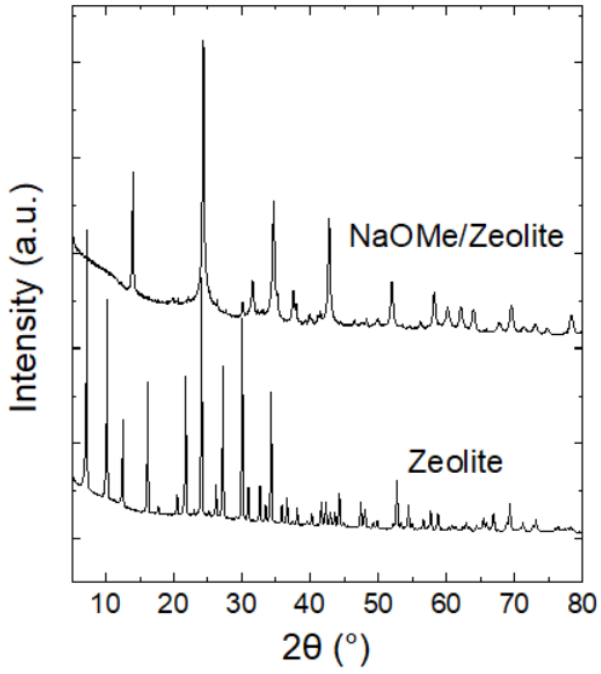

Figure 2. XRD spectrum of ball-milled NaOMe/zeolite catalyst in comparison to zeolite Y.

2.1.3. BET Surface Area

The surface area, half pore size, and cumulative pore volume of the zeolite Y and NaOMe/zeolite catalysts are shown in Table 1. It is observed that the BET surface area of zeolite Y, at 194.8 m^2/g, was reduced to 157.3 m^2/g for the NaOMe/zeolite catalyst. As the catalyst was prepared by a solvent-free ball-milling process, the NaOMe can block the micropores of zeolite Y, reducing the surface area. In addition, the reduced surface area is also due to the presence of NaOMe inside the macropores of zeolite Y [26,34]. This is also supported by the increased pore size for NaOMe/zeolite (5.692 Å) compared to zeolite Y (4.939 Å), as well as the decreased cumulative pore volume for NaOMe/zeolite (0.606 cm^3/g) compared to that of zeolite Y (0.655 cm^3/g). These are according to zeolite-doped catalyzed reactions [35]. Figure 3 shows the cumulative pore volume versus the half-pore width of both the zeolite Y and NaOMe/zeolite catalyst. We can see that the cumulative pore volume gradually increased from 2.8×10^{-4} $cm^3/g/nm$ to 3.8×10^{-4} $cm^3/g/nm$ at a half-pore width of about 37 Å for zeolite Y and NaOMe/zeolite, respectively. After 37 Å, there is a steady decrease in cumulative pore volume with the half-pore width. It is observed that the highest cumulative pore volume is assigned a half-pore width of 30–40 Å, whereas the pore volume drastically decreases after a half-pore width of 60 Å.

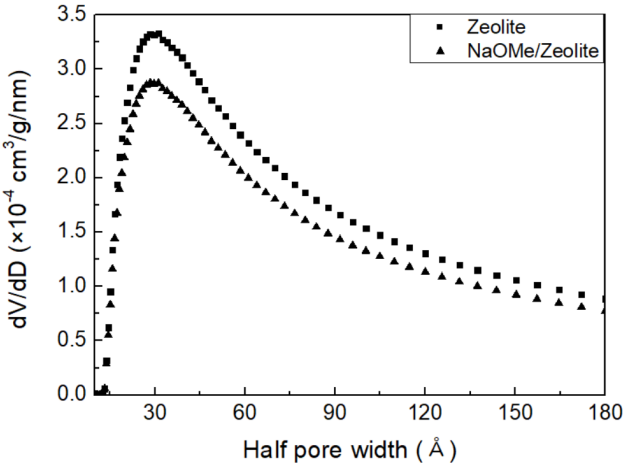

Figure 3. Graph of the BET surface area and cumulative pore volume to half−pore width.

Table 1. BET surface area analysis of zeolite Y and NaOMe/zeolite catalysts.

Characterization Technique	Zeolite	NaOMe/Zeolite
BET surface	194.780 m^2/g	157.274 m^2/g
Pore volume	0.6551 cm^3/g	0.606 cm^3/g
Pore size	4.939 Å	5.692 Å
DFT pore volume	0.159 cm^3/g	0.139 cm^3/g
DFT surface area	62.989 m^2/g	54.489 m^2/g
Half pore width	15.846 Å	15.846 Å

2.1.4. Scanning Electron Microscopy (SEM)

SEM images were captured to analyze the morphology of the catalyst and its components. The wt% of the chemical components in zeolite Y and NaOMe/zeolite are shown in Table 2. It can be seen that the wt% of carbon and sodium was drastically increased in the NaOMe/zeolite catalyst compared to zeolite Y, suggesting the optimum doping of sodium methoxide inside the pores of zeolite Y [36]. The SEM image of the zeolite Y used in catalyst synthesis is displayed in Figure 4, where its regular cubic shape can be observed [34,36]. Figure 5 shows SEM images of the NaOMe/zeolite catalyst synthesized

via ball milling. The difference in the structure of the catalyst and zeolite Y indicates the incorporation of NaOMe.

Table 2. Elemental analysis of raw zeolite and synthesized NaOMe/Zeolite catalyst.

Chemical Components	C	O	Na	Al	Si
Zeolite (wt%)	3.63	38.89	18.98	18.76	19.74
NaOMe/Zeolite (wt%)	11.66	40.89	33.41	6.82	7.21

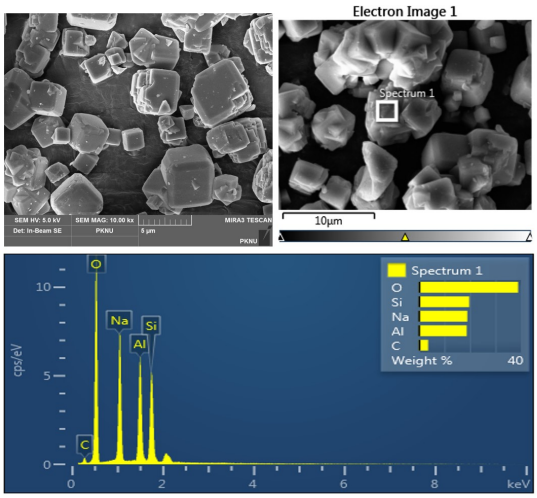

Figure 4. SEM image of zeolite.

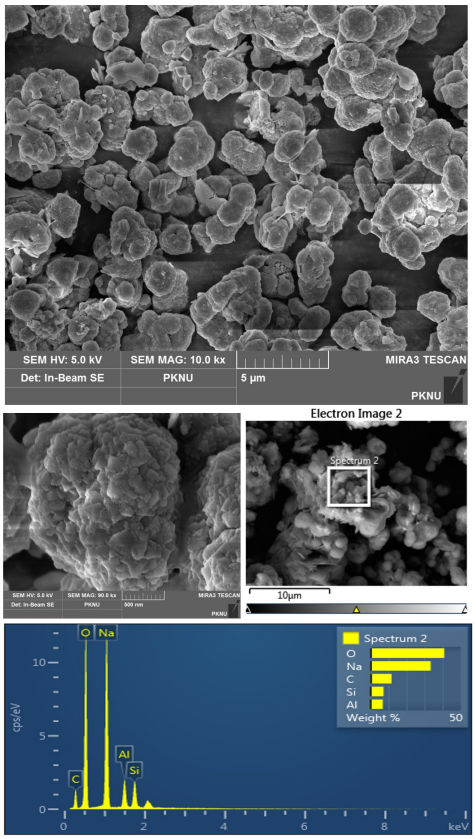

Figure 5. SEM images of NaOMe/zeolite catalyst synthesized via ball-milling process.

2.1.5. Transmission Electron Microscopy (TEM)

Figure 6 depicts the TEM image of the zeolite Y used to prepare the catalyst in which its hexagonal porous structure can be examined. The TEM image of the NaOMe/zeolite catalyst synthesized through ball milling is shown in Figure 7. It appears that the porous structure of zeolite Y is maintained in the catalyst with the incorporated sodium methoxide. Due to the outer surface area only being a small part of the total surface area, the majority of the active sites are inside the pores [36].

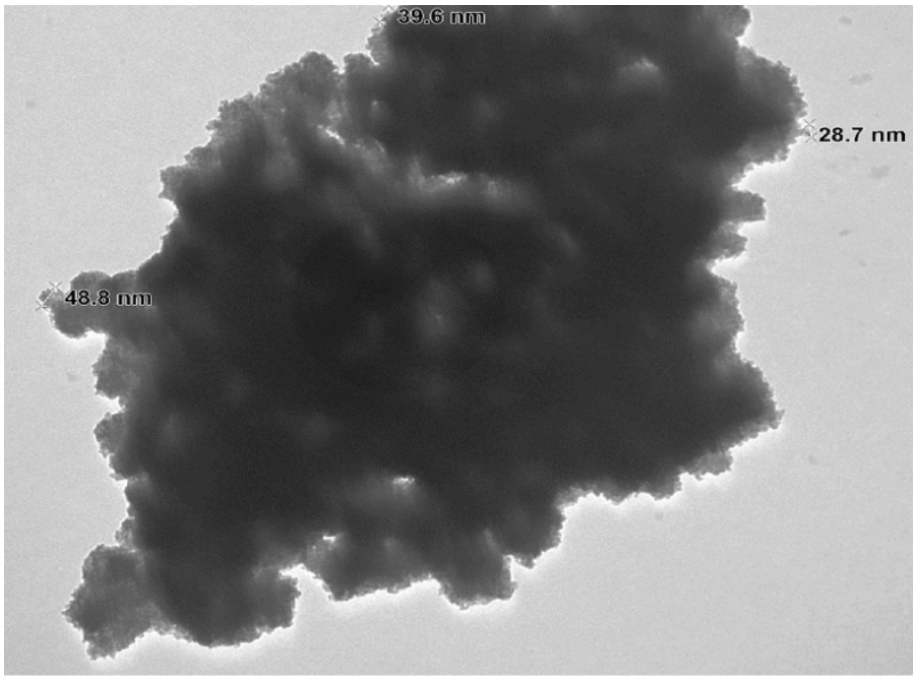

Figure 6. TEM image of zeolite.

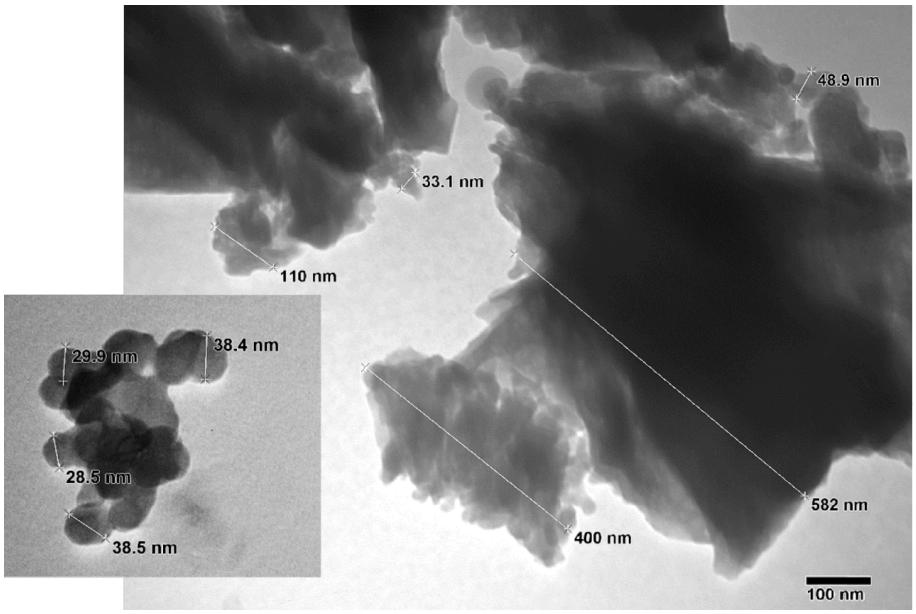

Figure 7. TEM image of NaOMe/zeolite catalyst synthesized via ball-milling process.

2.2. Catalytic Screening

To start with, we have synthesized a library of catalysts with NaOMe as one of the active reagents using a ball-milling process. Recent reports on the use of molybdenum oxide supported on Al_2O_3 for biodiesel production sparked our interest in using molybdenum/tungsten supported on titanium dioxide or clay [37]. However, the transesterification reaction of WCO using the above catalyst showed poor yield even after a 180 min reaction (Table 3). It was also observed that NaOMe ball milled with zeolite Y was found to be a promising catalyst for the transesterification of WCO. Moreover, blank tests were carried out with zeolite Y and NaOMe, which also resulted in a poor biodiesel yield. The products of these reactions can be seen in Figure 8.

Table 3. Catalyst screening for transesterification of WCO.

Sr. No.	Catalyst	Temp. (°C)	Oil/Methanol (Molar Ratio)	Time (min.)	Estimated Yield (%)
1	Zeolite	60	16:1	180	<10
2	NaOMe	60	16:1	180	91
3	NaOMe/zeolite	60	16:1	180	95

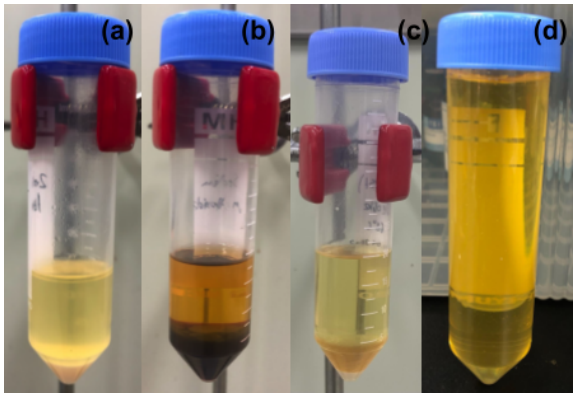

Figure 8. Phase-separated transesterification reaction mixture using catalysts: (**a**) zeolite, (**b**) NaOMe, (**c**) NaOMe/zeolite, (**d**) WCO.

2.3. Catalyst Activity

To determine the optimum conditions for the transesterification reaction, where the highest biodiesel yield is obtained and a clear product is formed with distinct phase separation, kinetic studies were conducted with the NaOMe/zeolite catalyst. These tests investigated the effect of several parameters, such as reaction time, reaction temperature, methanol volume, and the catalyst amount concentration, on the biodiesel yield. The results of our studies can be seen in the following graphs.

2.3.1. Effect of Methanol Volume on Biodiesel Yield

The biodiesel conversion of WCO as a function of the methanol volume used for transesterification can be seen in Figure 9. Biodiesel production was found to be above 95% with methanol volumes of $\geq$4 mL, and saponification was observed when $\leq$2 mL. An increase in the volume results in a higher biodiesel conversion due to it being necessary for the prevention of the reverse reaction [38]. This is akin to the trend observed with other catalysts [39]. At methanol volumes $\geq$5 mL, the biodiesel yield remains constant and is likely to decrease due to the excess methanol, which inactivates the catalyst and causes the reverse reaction to occur [33]. A yield of 96% was obtained with a methanol/oil ratio of 16:1; a similar result using other catalysts requires either significantly more heat or time [40,41].

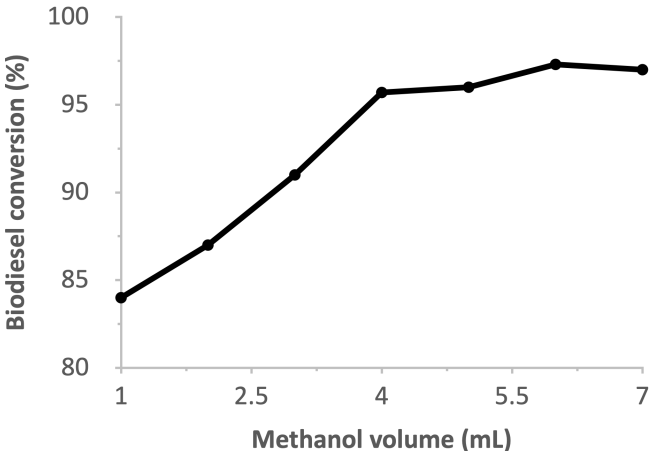

Figure 9. Effect of methanol volume on biodiesel conversion.

2.3.2. Effect of Catalyst Amount on Biodiesel Yield

Figure 10 shows the effect of wt% of NaOMe in Zeolite Y on the biodiesel yield. A very high yield was observed at 15 wt% and 20 wt% due to the increased number of active sites in the NaOMe/zeolite catalyst. As a homogeneous catalyst, 3–4 times the amount of NaOMe is needed to achieve a similar yield [28]. In our reaction, 0.289 g of catalyst was used, with a 2.1 wt% catalyst-to-WCO ratio, which means that only 0.058 g of NaOMe loaded on Zeolite Y. However, when a reaction was conducted individually with 0.058 g of NaOMe, the biodiesel yield drastically dropped to below 50%, suggesting the importance of NaOMe loading onto zeolite Y.

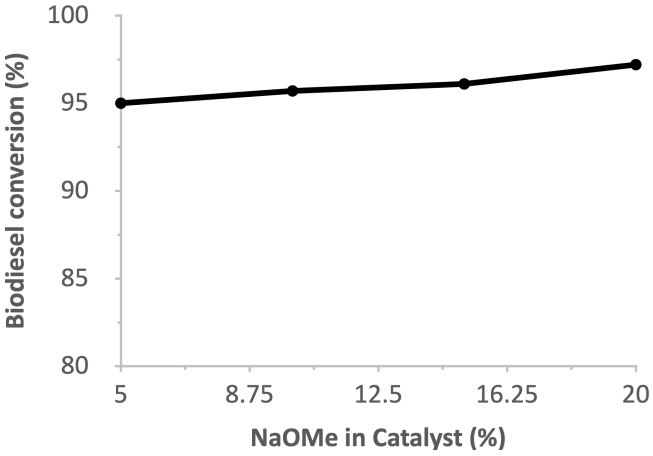

Figure 10. Effect of catalyst amount on biodiesel conversion.

2.3.3. Effect of Time on Biodiesel Yield

The effect of the reaction duration on the biodiesel conversion of the WCO can be observed in Figure 11. These tests were conducted under the following conditions: catalyst amount of 20%, methanol volume of 5 mL, and a temperature of 60 °C. The biodiesel yield remained relatively constant across the reaction times tested (30–180 min). This is likely due to the progressive decrease in the number of active sites available over the period of time as a result of catalyst deactivation [28,39]. At a duration of 30 min, we obtained a yield of 96.3%, and this can be considered optimum due to its cost-effectiveness and its comparatively higher biodiesel yield than other catalysts [42]. Furthermore, using a prolonged reaction time may cause saponification or the reverse reaction to occur, thereby reducing the WCO conversion [43].

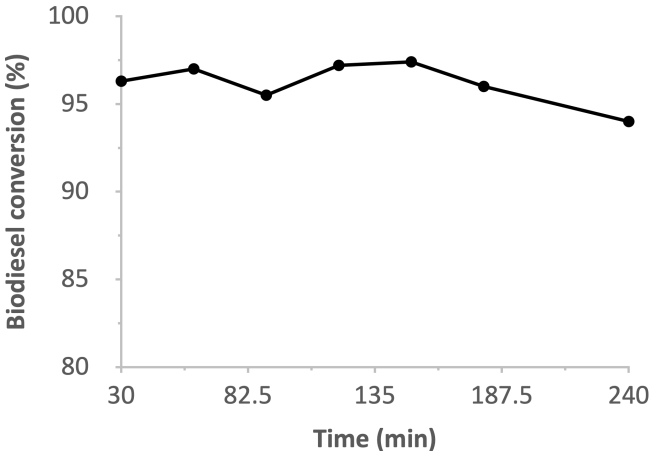

Figure 11. Effect of time on biodiesel conversion.

2.3.4. Effect of Temperature on Biodiesel Yield

In Figure 12, the influence of the reaction temperature on methyl ester biodiesel production is displayed. Biodiesel production is constant from 50–70 °C and decreased at 80 °C. This may be due to the evaporation of methanol, which is necessary for the interaction between WCO and the catalyst that leads to methyl ester conversion [44]. A corresponding increase is also observed in other transesterification reactions [29]. The NaOMe/zeolite catalyst at 60 °C showed a yield of about 97% in comparison to only zeolite Y as a catalyst with a yield of approximately 25% [28].

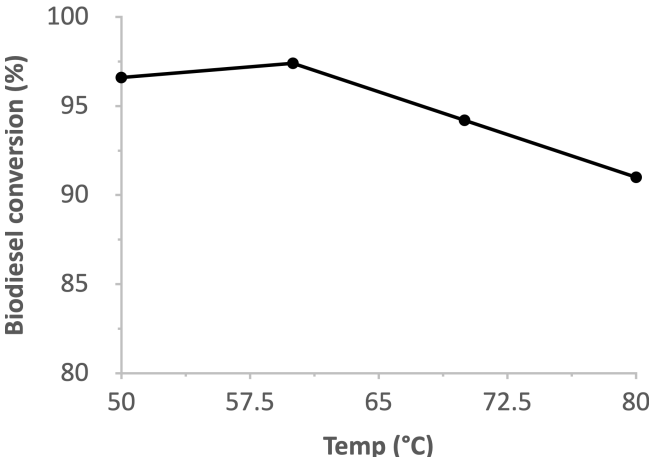

Figure 12. Effect of temperature on biodiesel conversion.

2.4. Plausible Mechanism of Transesterification of WCO

We made a couple of attempts to recycle the catalyst for the biodiesel reaction; however, the yield drastically dropped. This may lead to a misconception that the reaction is occurring in a homogeneous pathway. However, in most of the available references for NaOMe as a homogeneous catalyst, a 1–1.4 wt% NaOMe-to-oil ratio is required for a higher biodiesel yield. However, in our case, only a 0.4 wt% NaOMe (loaded on zeolite Y)-to-oil ratio is required to achieve a yield of about 95%. In addition, reports are available for zeolite Y as a catalyst with a yield of about 25% for biodiesel production [28]. Zeolite Y is well known for its surface hydroxyl groups [45]. These groups are supposed to react with sodium methoxide during the ball-milling process, resulting in the active sites for the transesterification reaction. Therefore, we believe that there is a cooperative mechanism between NaOMe and the surface of zeolite Y, resulting in the formation of active sites (Figure 13). There is a high possibility of catalyst deactivation because about a 3–4 times less amount of NaOMe was used for the catalyst preparation, hence resulting in fewer

active sites [28]. The plausible mechanism for the transesterification of WCO is given as follows in Figures 13 and 14 [46–48].

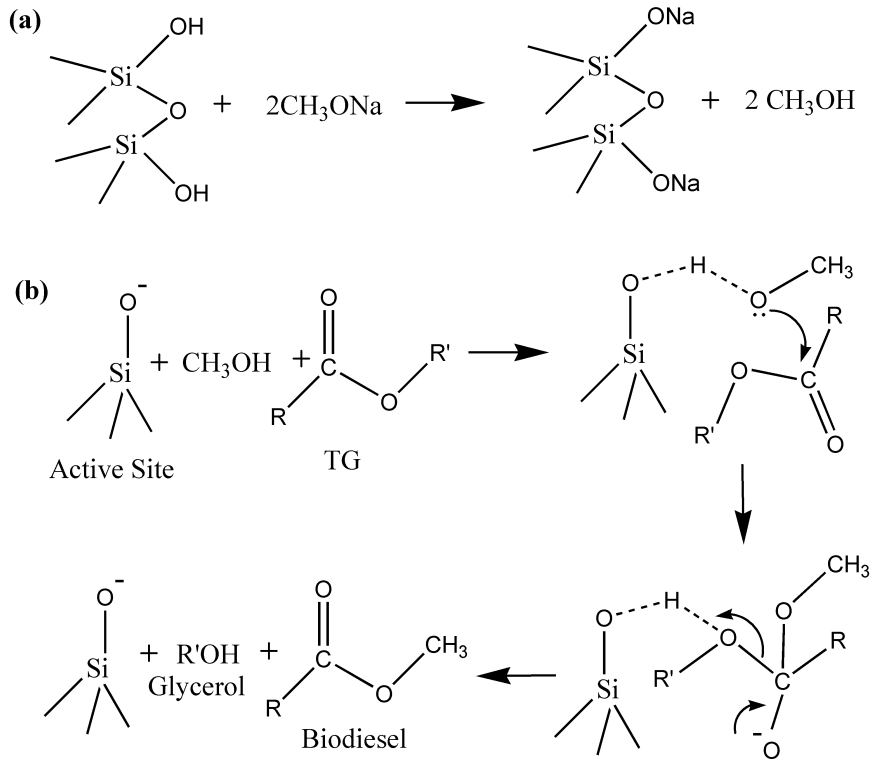

Figure 13. Plausible heterogeneous catalytic mechanisms: (**a**) Active site formation; (**b**) Transesterification of WCO using NaOMe/zeolite.

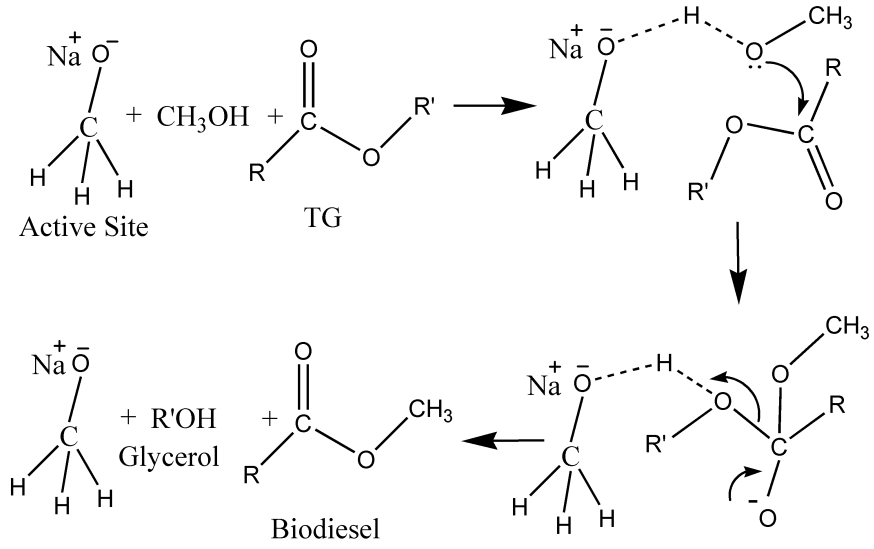

Figure 14. Plausible homogeneous catalytic mechanism of transesterification of WCO using NaOMe/zeolite.

2.5. Biodiesel Characterization

2.5.1. Fourier Transform Infrared Spectroscopy (FT−IR)

Figure 15 shows the Fourier transform infrared spectra of WCO, the raw biodiesel, and the raw glycerol. The FT−IR, as shown in the figure, was obtained in the range of 650–4000 cm^{-1} with 5 cm^{-1} resolution. Siatis et al. and Mahamuni and Adewuyi have noted that there are certain regions in the spectra of soybean oil and biodiesel

that show a slight difference [49,50]. Specifically, peaks in the 1425–1447 cm^{-1} and 1188–1200 cm^{-1} ranges are present in biodiesel spectra but not in oil spectra, while regions in the 1370–1400 cm^{-1} and 1075–1111 cm^{-1} ranges are present in soybean oil spectra but absent in biodiesel spectra. The authors also mentioned other regions in the spectra, such as the 1700–1800 cm^{-1} range corresponding to the C=O bond and the 2800–3000 cm^{-1} range corresponding to the CH stretching mode of olefins. The bending and oscillation vibrations corresponding to the -OCH_3 group are observed at 1436 cm^{-1} for the biodiesel but not for the WCO as triglycerides possess -OCH_2 and O-CH groups [51]. The peak at 1171 cm^{-1} in the biodiesel spectrum is associated with the stretching vibration of the C-O group attached to -CH_2, which is converted from the stretching vibration of the C-O group attached to -CH_2 seen in the WCO spectrum at 1160 cm^{-1} [52]. The absence of monoglyceride, diglyceride, glycerin, and methanol in the biodiesel can be determined due to the non-existent peak at 3200 cm^{-1}, which is associated with the -OH stretching vibration [51].

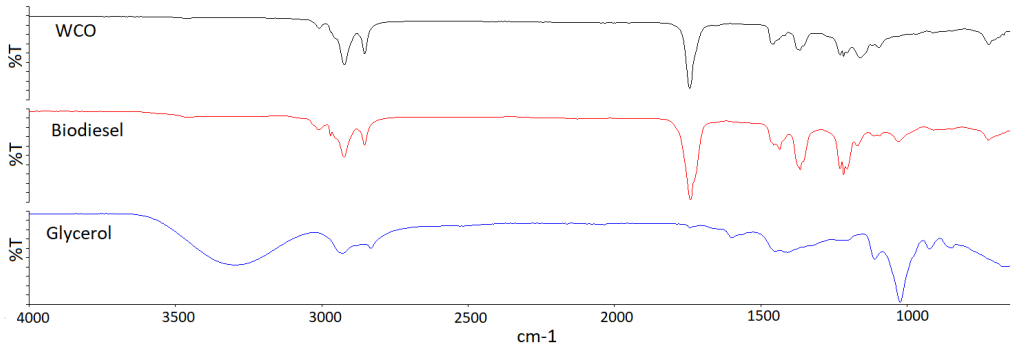

Figure 15. FT−IR spectrum of waste cooking oil in comparison to biodiesel and glycerol.

2.5.2. Nuclear Magnetic Resonance (^{1}H-NMR)

The nuclear magnetic resonance of ^{1}H-nuclei was assessed with 10–20 mg of WCO (Figure 8d) dissolved in $CDCl_3$. The FT-NMR spectra were recorded on a JEOL/JNMECZ-400 at room temperature. The WCO ^{1}H-NMR, as shown in Figure 16, shows characteristic chemical shifts of a triglyceride backbone and carboxylic protons. Most importantly, the peaks for the methylenic protons of the glycerol can be seen at 4.1–4.3 ppm, as shown in the figure [51]. Figure 17 shows the ^{1}H-NMR of raw biodiesel collected from the upper layer of the sample (Figure 8c) and assessed in $CDCl_3$ at room temperature. Here, the appearance of the biodiesel (fatty acid methyl ester) peak at 3.6 ppm and a drastic decrease in the intensity of methylenic protons of glycerol at 4.1 ppm and 4.3 ppm confirms the transesterification product. The ^{1}H-NMR of glycerol collected from the bottom second layer (Figure 8c) is shown in Figure 18, which supports the transesterification reaction of the WCO.

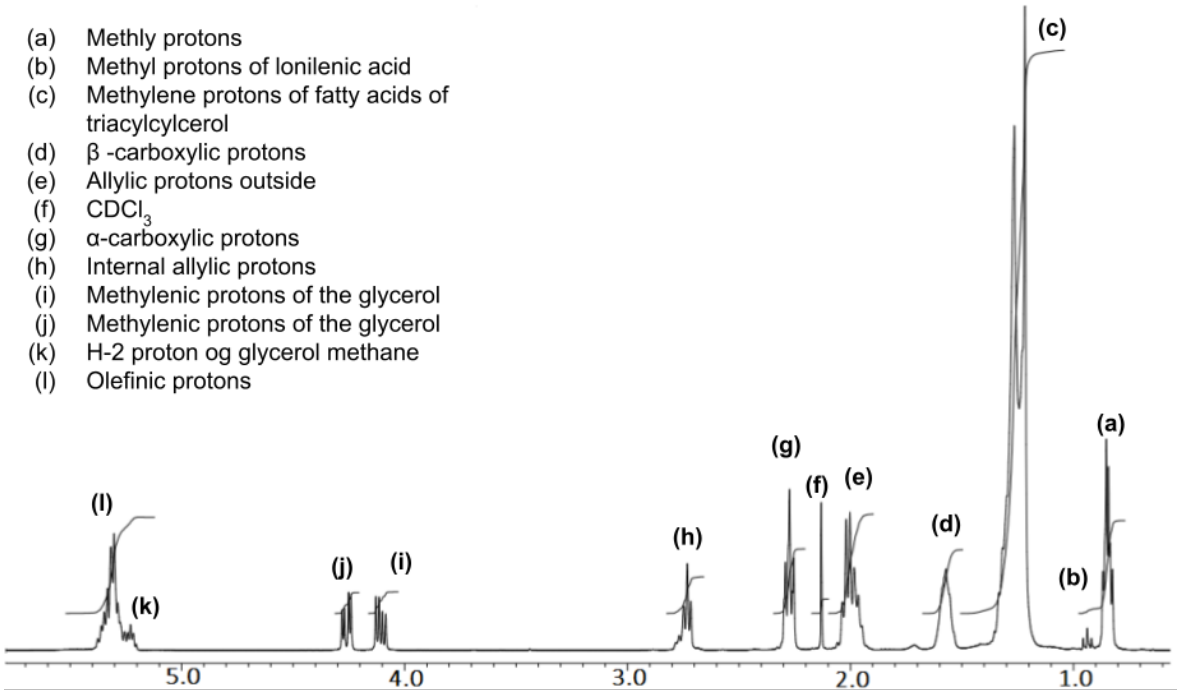

Figure 16. ^{1}H-NMR spectrum of waste cooking oil(WCO) in $CDCl_3$.

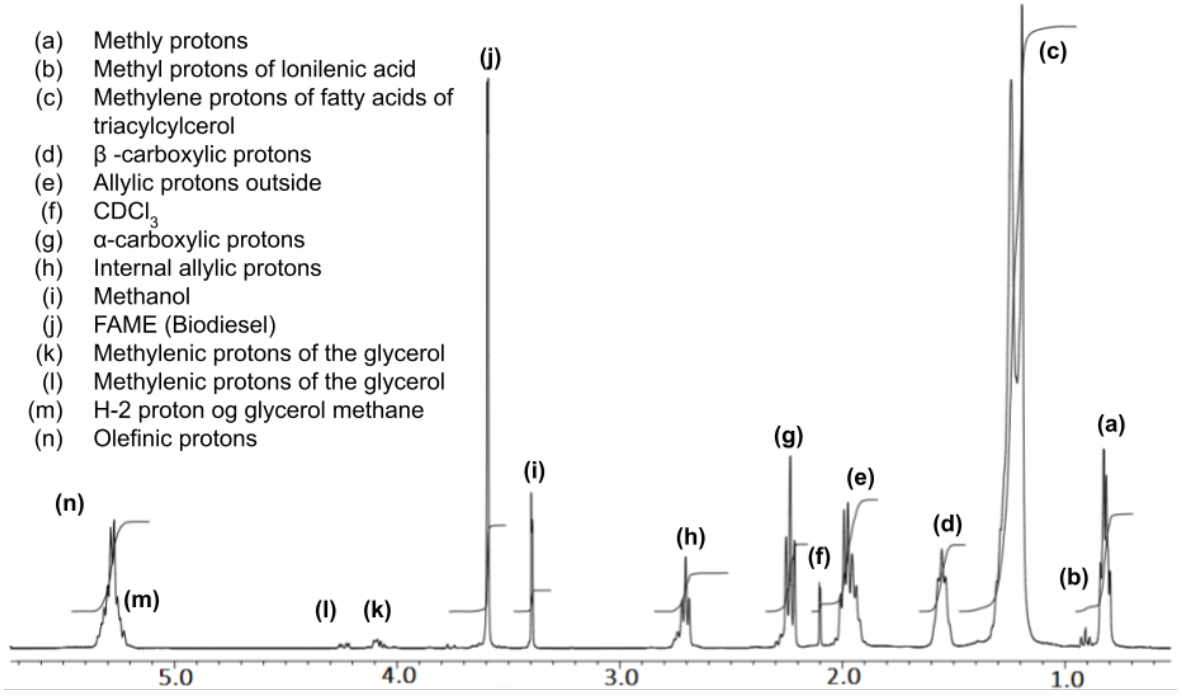

Figure 17. ^{1}H-NMR spectrum of phase-separated biodiesel in $CDCl_3$.

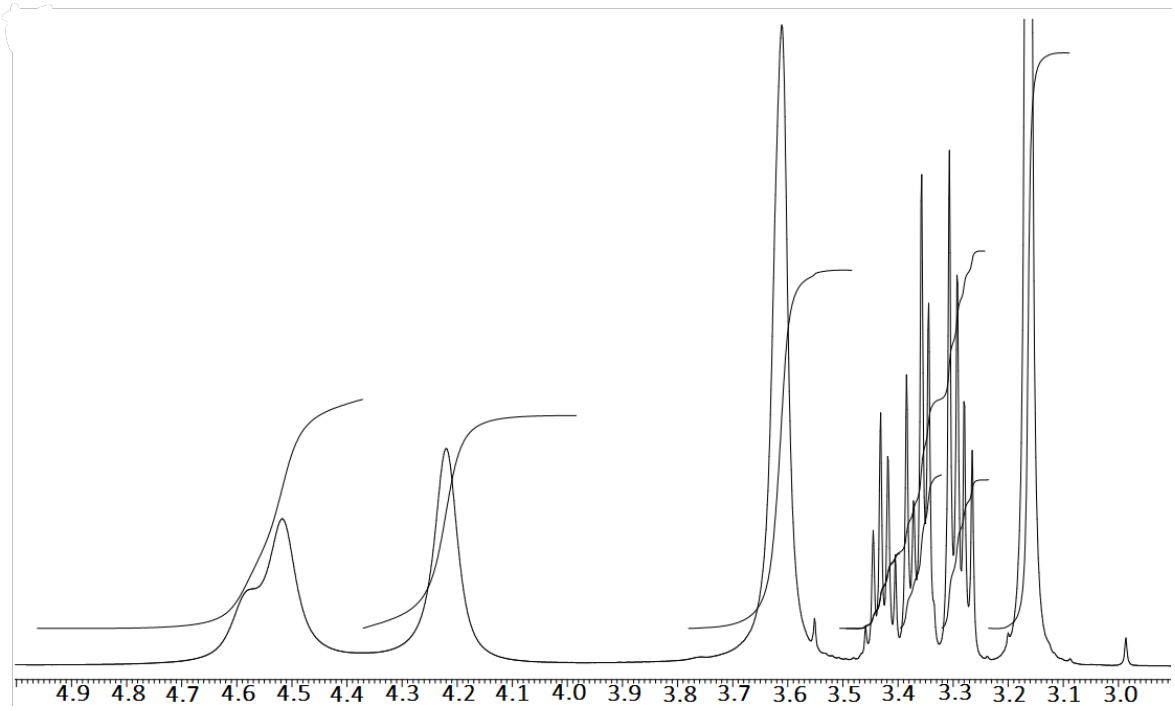

Figure 18. ^{1}H-NMR spectrum of phase-separated raw glycerol in D_2O.

2.5.3. Viscosity

The kinetic viscosity of the sample measures the internal resistance of the fluid under gravitational force. The viscosity arises from a near-surface velocity gradient in the turbulent region giving rise to larger viscous shear stresses in the biodiesel. One of the simple ways of calculating viscosity involves using a CANNON-FENSKE glass capillary viscometer. The viscosity can be obtained as a product of the flow time with the capillary constant of the viscometer. Based on the guidelines set by the ASTM standard, the viscosity values for biodiesel should range from 3 mm^2/s to 5.5 mm^2/s. The biodiesel produced (Figure 9c) using the NaOMe/zeolite catalyst showed a kinetic viscosity of 5.106 mm^2/s (Table 4), which falls within the above-mentioned standard [53].

Table 4. Viscosity measurement by using CANNON-FENSKE Viscometer.

Sample	Flow Time (sec.)			Meantime (Δt) sec.	K	Viscosity (mm^2/s) (v = KΔt)
	1	2	3			
Biodiesel	1255.3	1277.63	1296.77	1276.57	0.004	5.10628

3. Materials and Methods

3.1. Materials

All the materials were purchased from Sigma-Aldrich and used directly without further purification. The zeolite Y (BET surface area = 194.780 m^2/g, pore size = 4.939 Å, Si/Al = 31, NaY) and sodium methoxide (95% powder) were purchased from Sigma-Aldrich and used without additional treatment. Soybean waste cooking oil was collected from our school cafeteria and was previously used for the frying and cooking of different meals. After it was collected, it was then filtered with a sieve whose pore size was 50 µm to remove the suspended food particles from the raw oil. It was then heated to 110 °C for 6 h to remove moisture.

3.2. Catlayst Preparation

The catalyst was prepared by a solvent-free ball-milling process applied to the zeolite Y with powdered NaOMe for 6 h in a Samheung Energy ball miller (SH-Ball700-1) [54].

The ball milling was carried out using silica beads of 2 mm diameter for a given time period. The process was explicitly used to increase the surface area of the catalyst to enhance the catalytic yield. The NaOMe loading onto the zeolite Y was carried out in the range of 5–20% with 5% loading intervals at room temperature at 350 rpm for 6 h. The catalyst was then further characterized by SEM, TEM, XRD, BET surface area, and FT−IR analyses. The powder diffraction patterns of zeolite Y and NaOMe/zeolite were scanned using XRD in the 2θ range between 5 and 80° at a scanning speed of 5 °/min using a Cu-Kα radiation source of wavelength 1.5406 Å. The ball-milled catalyst surface area and pore analysis were carried out using a Quantachrome/Autosorb-Q instrument. To observe the surface structure of the NaOMe/zeolite, a field emission SEM–Schottky-type model TESCAN-MMIRA3 LMH was used. The nanostructure of the catalyst was assessed on a Hitachi TEM model-7600 with a magnification of 600,000×. The crystal structure of the above catalyst was analyzed on a Rijuku/UltimaIV XRD instrument. The vibrational stretching frequencies of the catalyst components were assessed using a PerkinElmer Frontier FT−IR spectrometer instrument with a Universal ATR Sampling Accessory.

3.3. Transesterification Procedure

The transesterification process was carried out in a 2-neck 100 mL round-bottom flask (RBF) equipped with a reflux facility and a digital thermometer in a hot silica oil bath maintained at a desired temperature. In a typical reaction, 0.289 g of NaOMe/zeolite catalyst (20% NaOMe loading) was transferred to 2-neck 100 mL RBF with a magnetic bar. A total of 5 mL of anhydrous methanol (methanol/oil molar ratio of 16:1) was then added to it and stirred for 20 min at room temperature. Finally, 14 g of WCO was added to the reaction mixture at the desired temperature and allowed to react for the next 30 min. After the reaction, the mixture was transferred to a 50 mL centrifuge tube and allowed to phase separate. Three distinct phases, where the topmost was biodiesel, the next was glycerol, and the bottom was the catalyst, were observed in the next 30 min. All these products were further characterized by FT−IR, ^{1}H-NMR, and viscosity measurements. The ^{1}H FT-NMR analysis of the WCO and transesterification product was done with a JEOL/JNMECZ-400 at room temperature. The FT−IR was obtained in the region of 650–4000 using a PerkinElmer Frontier FT−IR spectrometer instrument with a Universal ATR Sampling Accessory cm^{-1} with 5 cm^{-1} of resolution. The catalytic yield was calculated according to the reported literature in [55].

$$Biodiesel\ yield(\%) = \frac{Weight\ of\ biodiesel}{Weight\ of\ oil} \times 100 \quad (1)$$

4. Conclusions

The tests conducted in this study have presented a new catalyst for the conversion of WCO to biodiesel. The catalyst is a composition of NaOMe doped onto zeolite Y that is synthesized via a cost-effective and solvent-free ball-milling process with 20 wt% NaOMe loading onto zeolite. The study reveals that just a 0.4 wt% NaOMe-to-WCO ratio is required for the transesterification reaction with phase separation within 30 min. The kinetic studies revealed that a maximum biodiesel yield of 99% was attained with the optimum conditions of 20 wt% NaOMe loading, 5 mL of methanol (oil/methanol molar ratio of 16:1), 30 min reaction time, and a temperature of 60 °C. Several characterization procedures such as FT−IR, XRD, TEM, and FE-SEM were performed on the catalyst to ensure the incorporation of NaOMe into the zeolite Y pores, which is supported by a decrease in the surface area and an increased pore volume for the NaOMe/zeolite catalyst as a result of the ball-milling process. This is also confirmed by the SEM images. Finally, the formation of the biodiesel was confirmed by the ^{1}H-NMR and FT−IR of the raw phase-separated biodiesel, glycerol, and original WCO.

Author Contributions: Conceptualization, N.H.T.; Methodology, K.A.S. and J.M.M.; Software, E.-Y.C. and E.Y.; Validation, E.-Y.C.; Formal analysis, J.M.M. and E..Y.; Data curation, K.A.S. Writing—review & editing, E.-Y.C. and N.H.T. Visualization, E.-Y.C.; Supervision, N.H.T.; Project administration, N.H.T. All authors have read and agreed to the published version of the manuscript.

Funding: This work was supported by the Korea Science Academy of KAIST with funds from the Ministry of Science and ICT in Korea.

Data Availability Statement: Not applicable.

Conflicts of Interest: The authors declare no conflict of interest.

References

1. Oerther, S.E.; Rosa, W.E. Advocating for equality: The backbone of the sustainable development goals. *Am. J. Nurs.* **2020**, *120*, 60. [CrossRef] [PubMed]
2. IEA. IEA Key World Energy Statistics 2021—Analysis, IEA. Available online: https://www.iea.org/reports/key-world-energy-statistics-2021 (accessed on 8 April 2023).
3. Degfie, T.A.; Mamo, T.T.; Mekonnen, Y.S. Optimized Biodiesel Production from Waste Cooking Oil (WCO) Using Calcium Oxide (Cao) Nano-Catalyst. *Sci. Rep.* **2019**, *9*, 18982. [CrossRef] [PubMed]
4. Jaichandar, S.; Annamalai, K. The status of biodiesel as an alternative fuel for diesel engine—An overview. *J. Sustain. Energy Environ.* **2011**, *2*, 71–75.
5. Encinar, J.M.; González, J.F.; Sabio, E.; Ramiro, M.J. Preparation and properties of biodiesel from *Cynara cardunculus* L. oil. *Ind. Eng. Chem. Res.* **1999**, *38*, 2927–2931. [CrossRef]
6. Marchetti, J.M.; Miguel, V.U.; Errazu, A.F. Possible methods for biodiesel production. *Renew. Sustain. Energy Rev.* **2007**, *11*, 1300–1311. [CrossRef]
7. Notz, R.J.; Toennies, I.; McCann, N.; Scheffknecht, G.; Hasse, H. CO_2 Capture for Fossil Fuel-Fired Power Plants. *Chem. Eng. Technol.* **2011**, *34*, 163–172. [CrossRef]
8. Joshi, J.R.; Bheri, K.K.; Patel, J.V. Waste cooking oil as a promising source for bio lubricants—A review. *J. Indian Chem. Soc.* **2022**, *100*, 100820. [CrossRef]
9. Kulkarni, M.G.; Dalai, A.K. Waste cooking oil an economical source for biodiesel: A review. *Ind. Eng. Chem. Res.* **2006**, *45*, 2901–2913. [CrossRef]
10. Islam, A.; Taufiq-Yap, Y.H. *Advanced Technologies in Biodiesel: New Advances in Designed and Optimized Catalysts*; Momentum Press: New York, NY, USA, 2015.
11. Bezergianni, S.; Dimitriadis, A.; Kalogianni, A.; Pilavachi, P.A. Hydrotreating of waste cooking oil for biodiesel production. Part I: Effect of temperature on product yields and heteroatom removal. *Bioresour. Technol.* **2010**, *101*, 6651–6656. [CrossRef]
12. Bezergianni, S.; Dimitriadis, A.; Sfetsas, T.; Kalogianni, A. Hydrotreating of waste cooking oil for biodiesel production. Part II: Effect of temperature on hydrocarbon composition. *Bioresour. Technol.* **2010**, *101*, 7658–7660. [CrossRef]
13. Wang, S.; Zhang, Z.; Hou, X.; Lv, J.; Lan, G.; Yang, G.; Hu, J. The environmental potential of hydrogen addition as complementation for diesel and biodiesel: A comprehensive review and perspectives. *Fuel* **2023**, *342*, 127794. [CrossRef]
14. Tan, Y.H.; Abdullah, M.O.; Nolasco Hipolito, C. Comparison of biodiesel production between homogeneous and heterogeneous base catalysts. *Appl. Mech. Mater.* **2016**, *833*, 71–77. [CrossRef]
15. Rafati, A.; Tahvildari, K.; Nozari, M. Production of biodiesel by electrolysis method from waste cooking oil using heterogeneous MgO-NaOH nano catalyst. *Energy Sources Part Recover. Util. Environ. Eff.* **2018**, *41*, 1062–1074. [CrossRef]
16. Brito, A.; Borges, M.E.; Otero, N. Zeolite y as a Heterogeneous Catalyst in Biodiesel Fuel Production from Used Vegetable Oil. *Energy Fuels* **2007**, *21*, 3280–3283. [CrossRef]
17. Changmai, B.; Vanlalveni, C.; Ingle, A.P.; Bhagat, R.; Rokhum, S.L. Widely Used Catalysts in Biodiesel Production: A Review. *RSC Adv.* **2020**, *10*, 41625–41679. [CrossRef]
18. de Lima, A.L.; Ronconi, C.M.; Mota, C.J. Heterogeneous basic catalysts for biodiesel production. *Catal. Sci. Technol.* **2016**, *6*, 2877–2891. [CrossRef]
19. Melero, J.A.; Iglesias, J.; Morales, G. Heterogeneous acid catalysts for biodiesel production: Current status and future challenges. *Green Chem.* **2009**, *11*, 1285–1308. [CrossRef]
20. Bekele, D.T.; Shibeshi, N.T.; Reshad, A.S. Kno3-Loaded Coffee Husk Ash as a Heterogeneous Alkali Catalyst for Waste Frying Oil Valorization into Biodiesel. *ACS Omega* **2022**, *7*, 45129–45143. [CrossRef]
21. Valente, O.S.; Pasa, V.M.D.; Belchior, C.R.P.; Sodré, J.R. Physical–chemical properties of waste cooking oil biodiesel and castor oil biodiesel blends. *Fuel* **2011**, *90*, 1700–1702. [CrossRef]
22. Asli, H.; Ahmadinia, E.; Zargar, M.; Karim, M.R. Investigation on physical properties of waste cooking oil–Rejuvenated bitumen binder. *Constr. Build. Mater.* **2012**, *37*, 398–405. [CrossRef]
23. Lin, D.; Mao, Z.; Feng, X.; Zhou, X.; Yan, H.; Zhu, H.; Liu, Y.; Chen, X.; Tuo, Y.; Peng, C.; et al. Kinetic insights into deoxygenation of vegetable oils to produce second-generation biodiesel. *Fuel* **2023**, *333*, 126416. [CrossRef]

24. Mateos, P.S.; Navas, M.B.; Morcelle, S.R.; Ruscitti, C.; Matkovic, S.R.; Briand, L.E. Insights in the biocatalyzed hydrolysis, esterification and transesterification of waste cooking oil with a vegetable lipase. *Catal. Today* **2021**, *372*, 211–219. [CrossRef]
25. Sasaki, Y.; Suzuki, T.; Takamura, Y.; Saji, A.; Saka, H. Structure analysis of the mesopore in dealuminated zeolite Y by high resolution TEM observation with slow scan CCD camera. *J. Catal.* **1998**, *178*, 94–100. [CrossRef]
26. Qin, Z.; Wang, B.; Asano, N.; Wang, L.; Zhou, Y.; Liu, X.; Shen, B.; Mintova, S.; Asahina, S.; Valtchev, V. Towards a comprehensive understanding of mesoporosity in zeolite Y at the single particle level. *Inorg. Chem. Front.* **2022**, *9*, 2365–2373. [CrossRef]
27. Otieno, S.; Kengara, F.; Kowenje, C.; Mokaya, R. Optimization of Biodiesel Synthesis from Jatropha Curcas Oil Using Kaolin Derived zeolite Na–X as a Catalyst. *RSC Adv.* **2022**, *12*, 22792–22805. [CrossRef] [PubMed]
28. Nnaji, J.C. Advances in biodiesel synthesis: The role of various catalysts. *Open J. Eng. Sci.* **2020**, *1*, 53–71. [CrossRef]
29. Pikula, K.; Zakharenko, A.; Stratidakis, A.; Razgonova, M.; Nosyrev, A.; Mezhuev, Y.; Tsatsakis, A.; Golokhvast, K. The advances and limitations in biodiesel production: Feedstocks, oil extraction methods, production, and environmental life cycle assessment. *Green Chem. Lett. Rev.* **2020**, *13*, 275–294. [CrossRef]
30. Yin, H.; Zhou, T.; Liu, Y.; Chai, Y.; Liu, C. Synthesis of high-quality nanocrystalline zeolite Y using pseudoboehmite as aluminum source. *J. Porous Mater.* **2012**, *19*, 277–281. [CrossRef]
31. Rahman, M.M.; Awang, M.B.; Yusof, A.M. Preparation, characterization and application of zeolite-Y (Na-Y) for water filtration. *Aust. J. Basic Appl. Sci.* **2012**, *6*, 50–54.
32. Hashaikeh, R. Insight into Ball Milling for Size Reduction and Nanoparticles Production of H-y zeolite. *Mater. Chem. Phys.* **2018**, *220*, 322–330. [CrossRef]
33. Naik, B.D.; Meivelu, U. Experimental studies on sodium methoxide supported bentonite catalyst for biodiesel preparation from waste sunflower oil. *Environ. Prog. Sustain. Energy* **2020**, *39*, e13390. [CrossRef]
34. Travkina, O.S.; Agliullin, M.R.; Filippova, N.A.; Khazipova, A.N.; Danilova, I.G.; Grigor'Eva, N.G.; Narender, N.; Pavlov, M.L.; Kutepov, B.I. Template-free synthesis of high degree crystallinity zeolite Y with micro–meso–macroporous structure. *RSC Adv.* **2017**, *7*, 32581–32590. [CrossRef]
35. Ahmedzeki, N.S.; Yilmaz, S.; Al-Tabbakh, B.A. Synthesis and 459 Characterization of Nanocrystalline Zeolite Y. *Al-Khawarizmi Eng. J.* **2016**, *12*, 79–89.
36. Yokoi, T. Characterization of zeolites by advanced SEM/STEM techniques. *SI News* **2016**, *7*, 17–23.
37. Navajas, A.; Reyero, I.; Jiménez-Barrera, E.; Romero-Sarria, F.; Llorca, J.; Gandía, L.M. Catalytic Performance of Bulk and Al_2O_3-Supported Molybdenum Oxide for the Production of Biodiesel from Oil with High Free Fatty Acids Content. *Catalysts* **2020**, *10*, 158. [CrossRef]
38. Tarigan, J.B.; Singh, K.; Sinuraya, J.S.; Supeno, M.; Sembiring, H.; Tarigan, K.; Rambe, S.M.; Karo-Karo, J.A.; Sitepu, E.K. Waste Passion Fruit Peel as a Heterogeneous Catalyst for Room-Temperature Biodiesel Production. *ACS Omega* **2022**, *7*, 7885–7892. [CrossRef]
39. Erchamo, Y.S.; Mamo, T.T.; Workneh, G.A.; Mekonnen, Y.S. Improved Biodiesel Production from Waste Cooking 439 Oil with Mixed Methanol–Ethanol Using Enhanced Eggshell-Derived Cao Nano-Catalyst. *Sci. Rep.* **2021**, *11*, 6708. [CrossRef]
40. Enguilo Gonzaga, V.; Romero, R.; Gómez-Espinosa, R.M.; Romero, A.; Martínez, S.L.; Natividad, R. Biodiesel Production from Waste Cooking Oil Catalyzed by a Bifunctional Catalyst. *ACS Omega* **2021**, *6*, 24092–24105. [CrossRef]
41. Singh, D.; Sharma, D.; Soni, S.L.; Inda, C.S.; Sharma, S.; Sharma, P.K.; Jhalani, A. A Comprehensive Review of Biodiesel Production from Waste Cooking Oil and Its Use as Fuel in Compression Ignition Engines: 3rd Generation Cleaner Feedstock. *J. Clean. Prod.* **2021**, *307*, 127299. [CrossRef]
42. Yadav, G.; Ahmaruzzaman, M. Citrus Limetta Peel-Derived Catalyst for Sustainable Production of Biodiesel. *ACS Omega* **2022**, *7*, 28534–28544. [CrossRef]
43. Chanakaewsomboon, I.; Tongurai, C.; Photaworn, S.; Kungsanant, S.; Nikhom, R. Investigation of Saponification Mechanisms in Biodiesel Production: Microscopic Visualization of the Effects of FFA, Water and the Amount of Alkaline Catalyst. *J. Environ. Chem. Eng.* **2020**, *8*, 103538. [CrossRef]
44. Hameed, A.; Naqvi, S.R.; Sikandar, U.; Chen, W.-H. One-Step Biodiesel Production from Waste Cooking Oil Using CaO Promoted Activated Carbon Catalyst from Prunus persica Seeds. *Catalysts* **2022**, *12*, 592. [CrossRef]
45. Kianfar, E.; Hajimirzaee, S.; Mehr, A.S. Zeolite-Based Catalysts for Methanol to Gasoline Process: A Review. *Microchem. J.* **2020**, *156*, 104822. [CrossRef]
46. Taslim; Iskandinata, T.; Parinduri, I.; Ningsih, S.; Taruna, P.; Preparation, N. Characterization and application of natural zeolite from Tapanuli Indonesia modified with KOH as catalyst support for transesterification of rice bran oil. *Int. J. Eng. Res. Technol.* **2019**, *12*, 1474–1478.
47. Hsiao, M.C.; Kuo, J.Y.; Hsieh, P.H.; Hou, S.S. Improving Biodiesel Conversions from Blends of High- and Low-Acid-Value Waste Cooking Oils Using Sodium Methoxide as a Catalyst Based on a High Speed Homogenizer. *Energies* **2018**, *11*, 2298. [CrossRef]
48. Carlucci, C. An overview on the production of biodiesel enabled by continuous flow methodologies. *Catalysts* **2022**, *12*, 717. [CrossRef]
49. Siatis, N.G.; Kimbaris, A.C.; Pappas, C.S.; Tarantilis, P.A.; Polissiou, M.G. Improvement of Biodiesel Production Based on the Application of Ultrasound: Monitoring of the Procedure by FTIR Spectroscopy. *J. Am. Oil Chem. Soc.* **2006**, *83*, 53–57. [CrossRef]

50. Mahamuni, N.N.; Adewuyi, Y.G. Fourier Transform Infrared Spectroscopy (FTIR) Method to Monitor Soy Biodiesel and Soybean Oil in Transesterification Reactions, Petrodiesel-Biodiesel Blends, and Blend Adulteration with Soy Oil. *Energy Fuels* **2009**, *23*, 3773–3782. [CrossRef]
51. Ester, S.; Éder, S.; Rosa, O.; Sylvana, A.; Lauralice, C.; George, T. Use of nmr h 1 for physico-chemical properties of vegetable oils. In Proceedings of the 21st Brazilian Congress of Mechanical Engineering, Natal, Brazil, 24–28 October 2011.
52. Filali, N.; Slita, A.; Zakri, N.; Elazzouzi, H.; Rochdi, R.; El Joumani, M.; El Moussaoui, L.; Kabbaj, O.K.; Zrineh, A.; Kitane, S.; et al. CODEN (USA): PCHHAX Physical and chemical properties of biodiesel from fish oil. *Der Please Confirm. Pharma Chem.* **2016**, *8*, 15–17.
53. Measurement Substance Property-(tracomme.ch). Available online: https://www.tracomme.ch/wordpress/wp-content/uploads/2018/05/SI-Analytics_viscometers_E.pdf (accessed on 8 April 2023).
54. Fathinia, S.; Fathinia, M.; Rahmani, A.A.; Khataee, A. Preparation of natural pyrite nanoparticles by high energy planetary ball milling as a nanocatalyst for heterogeneous Fenton process. *Appl. Surf. Sci.* **2015**, *327*, 190–200. [CrossRef]
55. Takase, M. Biodiesel Yield and Conversion Percentage from Waste Frying Oil Using Fish Shell at Elmina as a Heterogeneous Catalyst and the Kinetics of the Reaction. *Int. J. Chem. Eng.* **2022**, *2022*, 8718638. [CrossRef]